

Ligand Effects on Optical Properties of Small Gold Clusters: A TDDFT Study

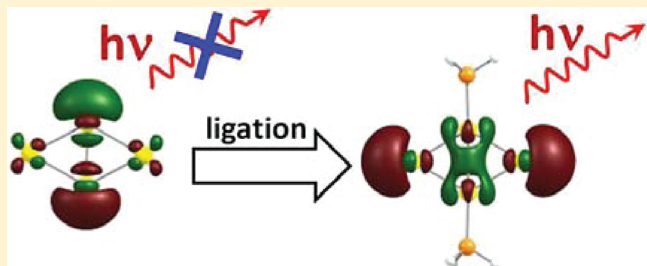
Satyender Goel,^{†,‡,||} Kirill A. Velizhanin,^{†,‡} Andrei Piryatinski,^{†,‡} Sergei A. Ivanov,^{§,*} and Sergei Tretiak^{†,‡,§,*}

[†]Theoretical Division, [‡]Center for Nonlinear Studies, [§]Center for Integrated Nano-Technologies, Los Alamos National Laboratory, New Mexico 87545, United States

^{||}NanoScience Technology Center, University of Central Florida, Orlando, Florida 32826, United States

Supporting Information

ABSTRACT: Ligand influence on the excited state structure of small neutral gold clusters (Au_2 and Au_4) has been investigated using Time Dependent Density Functional Theory. We study in detail the absorption profile of bare and ligated small gold clusters in solution modeled with Polarizable Continuum Model. Performance of CAM-B3LYP and TPSS DFT functionals combined with TZVP basis set has been assessed. We found that ligands substantially modify the excited state structure of clusters by eliminating low-lying optically inactive excited states. Depending on the ligand environment, the cluster may gain significant fluorescence efficiency. Our results suggest that small gold clusters ligated with amines will have better fluorescence potential compared to those ligated with phosphine or thiol ligands, in agreement with preliminary experimental data. TPSS fails to describe excited state structure of ligated clusters due to spurious charge-transfer states, thus highlighting the necessity of choosing appropriate quantum-chemistry model for correct excited state description.



INTRODUCTION

Ligated gold nanoparticles are potential candidates for numerous applications in the areas of modern technology and scientific advances, ranging from catalysis to molecular electronics and biological luminophores. As such, these applications have been the motivating factor behind the significant increase in research focused on the synthesis, characterization and theoretical analysis of small gold clusters, the building blocks of larger nanosize gold fragments. The gold nanoparticles, being biocompatible and relatively nontoxic, have attracted much attention during the past two decades owing to their size-dependent properties that are useful for applications like biosensors and optical materials.^{1,2}

Generally, the size-dependent optical properties of gold clusters have been a key factor to determine their structure in experiment.^{3–8} Precise control over quantum yield, absorption, and emission wavelength become critical in biolabeling and bioimaging applications, where the noble clusters may have the potential to replace semiconductor quantum dots.^{9,10} However, it was found difficult to determine precise chemical composition of optically active gold clusters in biological assemblies, since they potentially can contain inhomogeneous distribution of multiple cluster sizes and shapes in different ligand environments. Theory remains a complementary choice to gain an insight into structural makeup of clusters by simulating their structure–property relationships.

Previously, several experimental attempts have been made to explore the optical absorption and emission properties of small

gold clusters^{3–7,9–16} with the majority of them being bare metal clusters; to complement the experimental analysis, a variety of different theoretical chemistry methodologies has also been exploited.^{15,17–25} The wide interest in structural analysis of small noble metal clusters is driven by their attractive electronic properties. Although these molecular species show discrete electronic states and possible efficient fluorescence properties, only a few studies explored the optical absorption and emission properties of these clusters.^{5,7,9,26} In the investigation performed by Huang and Murray,²⁷ it is reported for gold nanoclusters with diameter above 1.5 nm that, although the monolayer of protecting ligands affect the efficiency and wavelength of the cluster phosphorescence, the emission energy still largely depends on the cluster core size. Recent review²⁸ provides detailed account on electronic structure of thiolated gold nanoclusters obtained with DFT methodology.

Cluster surface properties have been investigated with the adsorption of chemical species like NH_3 ,²⁹ CO ,³⁰ and organic molecules³¹ in order to get an insight into conjugated gold nanoparticles following their use in catalysis. Shafai et.al.³¹ report flattening of small gold 3D clusters due to adsorption of acetone molecule and formation of hydrogen bond between methyl group and gold atom. However, Kryachko and Remacle²⁹ reported bonding pattern of gold-ammonia

Received: September 9, 2011

Revised: January 4, 2012

Published: January 13, 2012

complexes in terms of an anchoring Au–N bond and nonconventional hydrogen bond with gold atom. Their work elucidates the issue of ligand influence on small gold clusters, albeit with an emphasis on the structural changes to the clusters in the presence of another molecule on their surface.

The potential use of gold clusters in opto-electronic and imaging applications requires further understanding of their optical properties in the presence of ligands and solvent to compliment experimental studies. A systematic work that explores optical properties of small gold clusters as a function of cluster geometry, ligand and solvent environment, is still lacking. We have recently³² reported the effect of solvent and ligation on the ground state structure and chemical energies of small gold clusters and outlined acceptable DFT based quantum chemistry models. Here, we extend our study to investigate optical properties of Au_2 and Au_4 clusters ligated with different types of donor ligands, with the emphasis on phosphines and amines.

■ COMPUTATIONAL APPROACH

All calculations have been performed using the commercially available Gaussian09³³ software package. Excited state structure and related optical properties of all molecules have been calculated with Time Dependent Density Functional Theory (TDDFT) methodology, which is currently the mainstream approach for quantitative modeling of electronic excitations in medium-sized molecules, including metallic and organometallic complexes. We use def2-TZVP, triple- ζ valence ECP basis set with polarization of Ahlrichs et al.³⁴ We also employ two recently developed DFT models, namely, the kinetic-energy density-dependent functional (meta-GGA) TPSS³⁵ and long-range corrected functional CAM-B3LYP³⁶ accounting for long-range exchange effects. Combination of TPSS functional and TZVP basis set allowed quantitative modeling of geometries and ligand binding energies in our previous work.³² As we discuss in this work, the use of CAM-B3LYP model is important for eliminating nonphysical charge transfer states that could be present in such systems with polar metal–ligand bonding. Detailed investigation of other DFT models and basis set effect on optical properties of gold clusters will be reported elsewhere. Here, we also limit our discussion to modeling in a solvent environment to mimic the respective experimental conditions. We note that solvent substantially modifies optical absorption of the ligated cluster which will also be discussed in detail in our future work. As such, all calculations have been performed with solvation effects simulated by using implicit CPCM solvation model³⁷ as implemented in Gaussian09 with methanol being a solvent of choice. The geometries were optimized at TPSS/TZVP level following our previous work.³² TDDFT calculations were then performed for the first 20 excited states with CAM-B3LYP/TZVP and TPSS/TZVP using TPSS/TZVP geometries. Finally, Natural Transition Orbital³⁸ (NTO) analysis has been conducted to understand the nature and properties of calculated excited states. GaussView(v3.0) and ChemCraft (v1.6) visualization software packages were used for subsequent visualization of resulting molecular structures and transition orbitals. The contribution of metal atomic orbitals into frontier NTOs was calculated using the *Fragment* option in Gaussian 09 and using NBO analysis of metal and ligand contribution to the Electron and Hole Transition Orbitals, ENTO and HNTO, respectively.

■ RESULTS AND DISCUSSION

Before analyzing optical properties, we first examine the Kohn–Sham orbital makeup of bare and amine-ligated Au_2 dimer presented in Figure 1. All molecular orbitals (MOs) of the

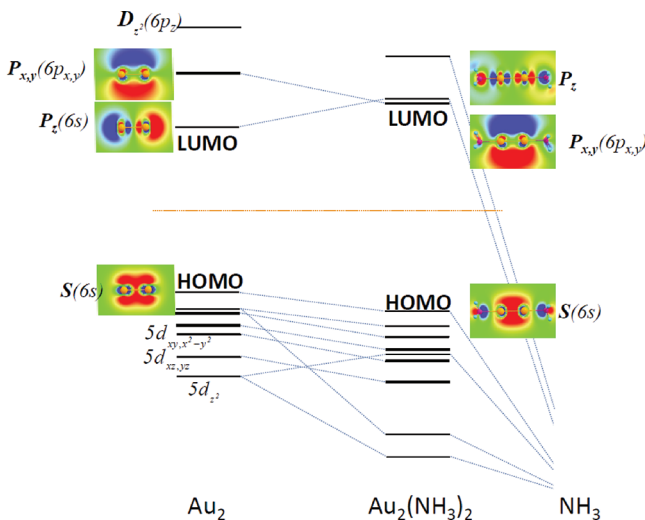


Figure 1. Diagram of frontier molecular orbitals of bare and NH_3 -stabilized Au_2 dimer.

studied clusters can be classified as a combination of 5d-band of gold and superatom (cluster) orbitals that are in great degree composed of gold 6s and 6p atomic orbitals (AOs) with certain degree of hybridization with a lone-pair (LP) of bonding ligands (see more detailed discussion below). The cluster orbital concept, in part, was introduced³⁹ to simplify the qualitative description of MOs of metal and borane clusters where each cluster orbital represents the combination of AOs with angular momentum symmetry resembling that of atomic orbitals: S, P, D, and so on. For the same reason of simplicity, the cluster orbital symbolics is used throughout the paper. Cluster orbitals are denoted with upper case bold letters corresponding to the orbital's angular momentum with AOs mainly contributing to cluster orbital being shown in parentheses.

As presented in Figure 1, the Highest Occupied Molecular Orbital (HOMO) of Au_2 dimer is S-type cluster orbital made up of bonding combination of gold 6s AOs, $S(6s)$, whereas the Lowest Unoccupied Molecular Orbital (LUMO) of the dimer is P_z -type cluster orbital (antibonding combination of gold 6s AOs), $P_z(6s)$. The LUMO+1 is doubly degenerate $P_{x,y}$ cluster orbital mostly composed of gold 6s and 6p AOs, $P_{x,y}(6sp)$. Thus, the ligation with two ammonia molecules stabilizes dimer's HOMO and LUMO+1 orbitals and destabilizes LUMO, causing the reordering of frontier orbitals, which has significant effect on optical spectra.

The following analysis of cluster optical properties is based on the assumption of Kasha's rule applicability to studied systems: system relaxes to the first excited state before emitting a photon. The rule's applicability to the majority of studied luminescent species justifies our assumption. As such, the nature of the lowest excitation is as important as the nature of the higher excited states with large oscillator strengths dominating optical absorption since the former will most likely determine the system's luminescent properties.

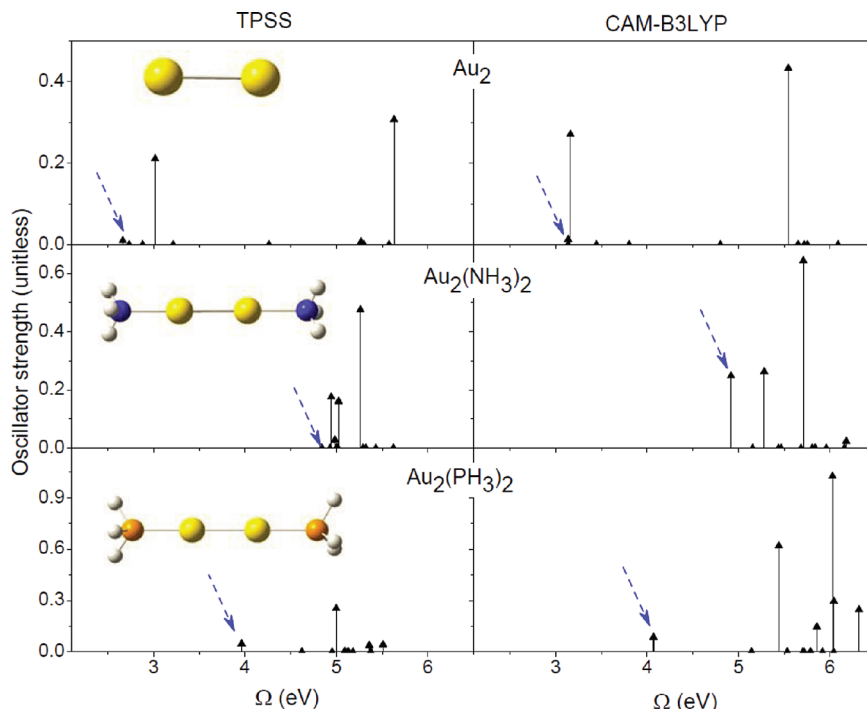


Figure 2. Absorption spectra of bare and ligated Au_2 . Spectra on the left (right) are calculated using TPSS (CAM-B3LYP) functional and TZVP basis set. The arrows indicate positions of the lowest absorption transitions. Molecular structures are shown in the insets.

Figures 2 and 3 present calculated absorption spectra of bare and ligated Au_2 and Au_4 clusters, respectively, using TDDFT methodology. We study the same set of molecules shown in Figures 2 and 3 insets as in our previous investigation of their ground state properties.³² Taking into account results of work by Balasubramanian,⁴⁰ we consider the rhombus geometry of the Au_4 cluster being the lowest energy isomer. In this section of theoretical analysis, two types of donor ligands, amine, and phosphine (modeled by NH_3 and PH_3 , respectively), that can be used in an experiment, have been used to construct three types of ligated clusters, Au_2L_2 , Au_4L_2 , and Au_4L_4 . Calculated optical absorption for each cluster is shown as “stick spectra” plots of the dimensionless oscillator strength f vs respective excitation energies Ω (Figures 2 and 3). To analyze the orbital makeup of the lowest electronic transition in the clusters, it is beneficial to consider cluster’s NTOs rather than MOs. Transition Orbitals represent the wave functions of an electron and a hole underlying a specific optical excitation. Notably that for many considered electronic excitations, the NTO analysis allows representation of each excited state through a single electron–hole pair with its contribution exceeding 98% to the related transition density matrix.³⁸ The lowest excited state (that may be relevant to the fluorescence) shown by blue arrows in Figures 2 and 3 for selected molecules, are displayed in Table 1. Additional NTO plots are given in Table S1 of the Supporting Information, SI. For the reference, we also present the Kohn–Sham orbital makeup of bare and ligated Au_4 cluster in Figure S1 of the SI.

Au_2 bare cluster shows two significant peaks in its optical absorption (Figure 2). The orbital makeup of these two transitions is detailed in Table 3 and Table S2 of the Supporting Information, SI. The lowest excited state is optically forbidden by symmetry in both CAM-B3LYP and TPSS methods. Given the large gap between the lowest dark state and the first optically active state, TPSS essentially predicts Au_2

cluster to be non- (or weakly) fluorescent, since in a majority of molecular systems, according to Kasha’s rule, optically allowed (or forbidden) lowest excited state well separated from the other states typically indicates possibility (or absence) of fluorescence. However, CAM-B3LYP places several lowest excited states (including optically allowed ones) to be nearly degenerate. Consequently, Au_2 can have efficient fluorescence through the oscillator strength borrowing or Franck–Condon activity mechanisms, which agrees with experimental emission data of Au_2 clusters in the argon matrix.^{41,42} Although HOMO and LUMO of bare Au_2 dimer can be represented as $S(6s)$ and $P_z(6s)$ cluster orbitals, the electron and hole NTOs (ENTO and HNTO) of this transition can be described as corresponding to $P_z(6s)$ cluster orbital (ENTO) and $P_z(5d,6s)$ cluster orbital (HNTO) (Table 1). However, the first four electronic transitions in Au_2 dimer are practically degenerate (with 0.015 eV difference between the first and the fourth transition) and the fourth transition (the lowest transition with high oscillator strength) can be ascribed to the $S(6s) \rightarrow P_z(6s)$ excitation. It appears that CAM-B3LYP treatment might not be fully adequate to describe the correct order of electronic transitions (see below) and one would need to use another DFT functional with *higher* Hartree–Fock contribution at long ranges, such as LC- ω PBE.⁴³ Indeed, the LC- ω PBE treatment of Au_2 dimer slightly decreases the energy of $S(6s) \rightarrow P_z(6s)$ making it the lowest electronic transition (more details in Table S2 of the SI).

To assess the influence of the type of a ligand on the nature of the lowest absorption transition in gold clusters, we have calculated energies and oscillator strengths of the lowest transition in the gold dimer Au_2L_2 ligated with series of donor ligands (Table 2). The ligands with O, N, S, and P donor atoms were considered spanning such classes of ligands as aliphatic and aromatic amines, phosphines and phosphine oxides, alcohols and esters with thio analogues, and carboxylic acids.

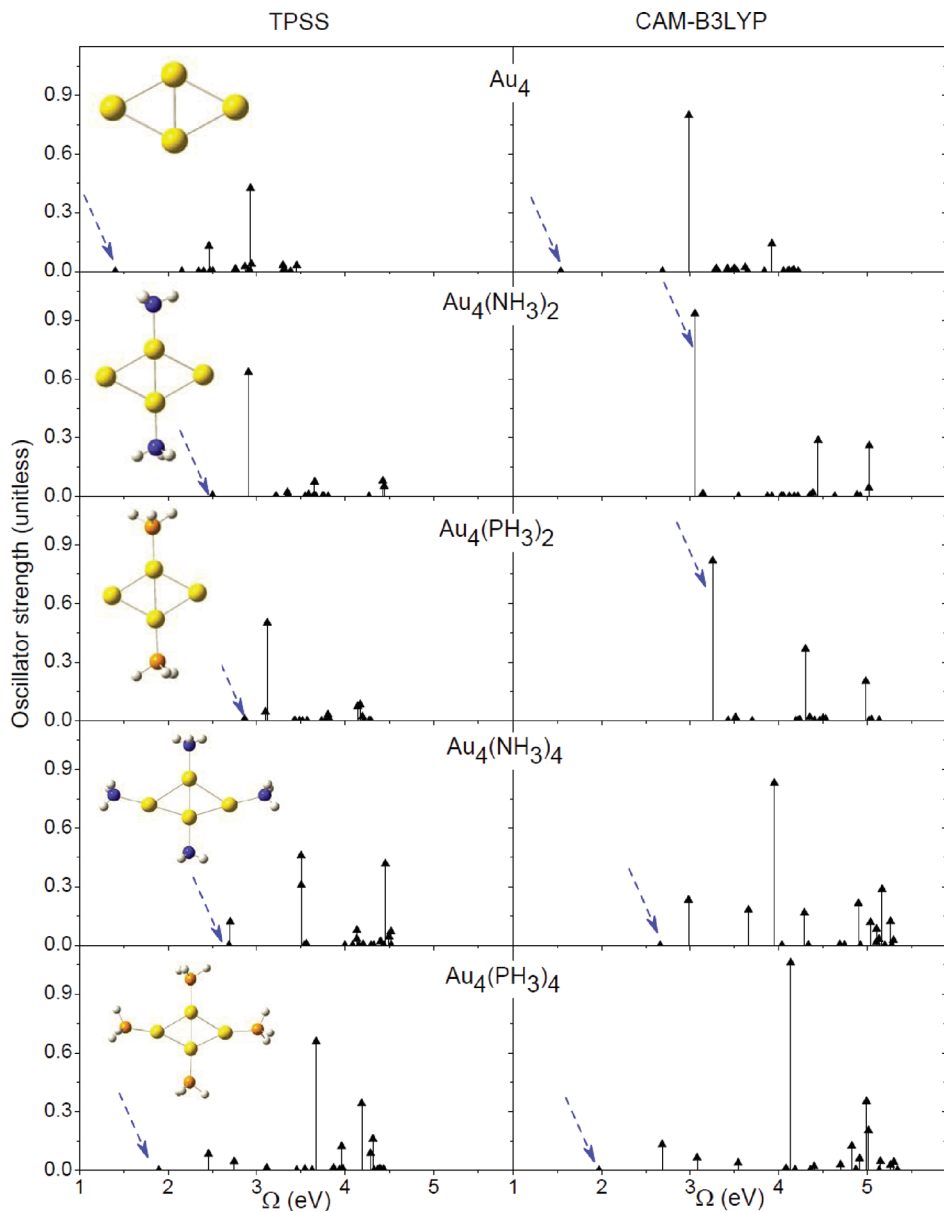


Figure 3. Same as Figure 2, but for Au_4 .

The second order perturbation analysis of Fock matrix (within NBO procedure) identified two main donor–acceptor interactions between Au_2 dimer and ligands: the electron donation from Lone Pair (LP) of ligand's donor atom onto the dimer's LUMO (which is antibonding with respect to $\text{Au}-\text{Au}$ interaction), and the electron donation from HOMO onto first Ry* orbital of the donor atom, which is composed of unoccupied *s* and *p* natural AOs of the atom. The LP \rightarrow LUMO donation is the main interaction responsible for the metal–ligand binding. This interaction is weak in case of ligands with oxygen, resulting in short $\text{Au}-\text{Au}$ bonding and increases as donor atom changes from O to N, S, and P, giving rise to longer $\text{Au}-\text{Au}$ bonds. Coordination of even such weak ligand as water appears enough to slightly reorder the electronic transitions causing the $\text{S}(6s) \rightarrow \text{P}_z(6s)$ excitation to become the lowest electronic transition (Table 2). At the same time, due to the bonding ligand–metal interaction, the energy and oscillator strength of the lowest transitions in ligated clusters becomes higher than in the bare dimer. However, because this

interaction is weak, it does not change the makeup of ENTO: the first transition still occurs into the $\text{P}_z(6p)$ orbital. The increase in electron donation from donor atom onto Au_2 dimer destabilizes the $\text{P}_z(6p)$ orbital, resulting in $\text{P}_{xy}(6p)$ becoming the main component of cluster's ENTO. At the same time, as the electronegativity of the donor atom decreases along the row $\text{N} > \text{S} > \text{P}$, the contribution of *ligand* atomic orbitals in ENTO and HNTO increases, that is clearly visible on the images of corresponding ENTO and HNTO orbitals. In turn, the delocalization of ENTO and HNTO onto ligands causes the drop in the oscillator strength of the first absorbing transition. The drop in this oscillator strength correlates with decreasing efficiency of the cluster emission, unless the delocalization of the excitation enables a unique route of radiative recombination from ligands onto the metal, as it appears to be happening in the case of large thiolated gold clusters, where $\text{Au}(\text{SR})_2^-$ and $\text{Au}_2(\text{SR})_3^-$ units on the cluster surface can be considered as ligand entities, protecting the positively charged cluster core.⁴⁴ However, even in the

Table 1. Electron and Hole Natural Transition orbitals, ENTO and HNTO, of Lowest Excited States in Bare and Ligated Au₂ and Au₄ Clusters^a

	ENTO	HNTO
Au ₂		
CAM-B3LYP 3.13 eV (0.00)		
TPSS 2.66 eV (0.01)		
Au ₂ (NH ₃) ₂		
CAM-B3LYP 4.92 eV (0.25)		
TPSS 4.84 eV (0.00)		
Au ₄		
CAM-B3LYP 1.54 eV (0.00)		
TPSS 1.40 eV (0.01)		
Au ₄ (PH ₃) ₂		
CAM-B3LYP 3.26 eV (0.82)		
TPSS 2.87 eV (0.01)		
Au ₄ (NH ₃) ₄		
CAM-B3LYP 2.66 eV (0.00)		
TPSS 2.69 eV (0.00)		

^aThe left column shows DFT functional used, the energy of the lowest transition and, in parentheses, its respective oscillator strength. Additional plots are given in the SI.

described case, the emission efficiency is expected to be low due to increased likelihood of ligand-assisted nonradiative relaxation that was also shown experimentally.⁴⁴

As indicated in the literature, the fluorescent gold clusters appear to require the presence of amines for efficient emission.⁴⁵ We believe that our results provide a theoretical justification to this experimental observation and point to the general trend that, given the correct symmetries of donor and acceptor orbitals, as the first transition gets *more localized* (or possesses less charge-transfer character), its absorption will increase, and, as a consequence, the cluster gains better emission potential. Since the lowest unoccupied orbitals tend to be composed primarily of gold 6s and 6p AOs combined into *P* cluster orbitals, in order to have an appropriate symmetry for high-intensity absorption transitions, the transition should originate from the *S* cluster orbital. Indeed, the strongest transitions in the absorption spectra of studied clusters can be assigned to be composed of mainly *S*→*P_z* or *S*→*P_{x,y}* excitations (Table 3 in the text and Tables S2 and S3 of the Supporting Information). It is also evident that the metal–ligand bond energy somewhat correlates with the degree of delocalization, and the strongest bound ligands (phosphines and thiols) are

also the least beneficial for cluster luminescence. Pyridine ligand appears as an exception to this trend since its binding is comparable to the rest of considered amines, but the oscillator strength of the transition in Au₂Py₂ is the lowest among analyzed clusters. The latter is due to a significant charge-transfer character of the first absorption transition, from the metal-localized HNTO onto the ligand-localized ENTO. In the case of fluorescent gold clusters, any hard ligand (such as ligands with nitrogen or oxygen donor atoms, e.g., H₂O) will ensure high oscillator strength of the first transition. It follows from these results that aqueous solutions might facilitate the higher emission efficiencies of neutral gold clusters. A limited experimental confirmation of this effect has been provided in the literature.⁴⁶ For the practical purposes of cluster stability, the high metal–ligand binding energy is also important. As such, we believe that amines are the best suited ligands to both stabilize the cluster and ensure its high fluorescence yield. Unlike the alkyl amines, conjugated amines, such as pyridine, would be very detrimental to cluster's emission, as the oscillator strength of the first transition is very small. In contrast, according to CAM-B3LYP calculations, the stabilization of the gold dimer with phosphines, strong and commonly used ligands in gold cluster chemistry, results solely in weakly absorbing/emissive excited state of Au₂(PH₃)₂ in the middle energy region, that is caused by the decreased overlap of electron and hole orbitals (see Tables 2 and S1 of the SI) compared to that of Au₂(NH₃)₂ cluster, thus rationalizing weak oscillator strength of the lowest transition in Au₂(PH₃)₂.

In TPSS modeling, the lowest excited state of Au₂(NH₃)₂ is optically inactive (see Figure 2) with electron and hole NTOs resembling *P_x* and *P_z* cluster orbitals, respectively (Table 1). This contradicts the CAM-B3LYP results and does not seem to agree with the experimental observation.^{45,47} We attribute this discrepancy to the artifacts of the semilocal DFT models (such as TPSS) prone to the improper description of charge-transfer states previously explored for different molecular systems.^{48,49} Since, by design, the long-range corrected DFT models (CAM-B3LYP or LC- ω PBE) should correctly describe the cases with charge-transfer nature, it justifies the attribution of the difference between TPSS and CAM-B3LYP results to such cases in studied systems herein. It is noteworthy that the lowest dark states of both Au₂ and Au₂(NH₃)₂ in the TPSS model have vanishing integral overlap between their electron and hole orbitals (Table 1), which renders these states to be optically forbidden. In other words, the absence of any overlap between NTO orbitals of low-lying excited states indicate its charge-transfer nature (in a general sense) and points to a possible fault of semilocal DFT models. Consequently, a TPSS approach places these optically forbidden states energetically too low in the ligated clusters, which is inconsistent with optically active states, for which the significant overlap exists between electron and hole orbitals. A similar situation is observed for ligated Au₄ clusters discussed below. Finally, the lowest excited state in Au₂(PH₃)₂ has similar energy in both TPSS and CAM-B3LYP models (Figure 2) although different NTO makeup (Tables 1 and 1S).

Similar behavior is observed for Au₄ cluster family in CAM-B3LYP modeling, however, with several unique differences. The first electronic transition of Au₄ cluster is significantly red-shifted from the other excited states (Figure 3). This state is optically dark (by symmetry) and can be represented in the NTO analysis (Table 1), primarily, as *P_z(6s)*→*P_x(6s)* transition from antibonding combination of two outer gold 6s

Table 2. Contribution of Gold AOs into Electron/Hole NTOs (in %) of the Lowest Electronic Transition, Energy Ω (eV) and Oscillator Strength f of the Transition; the Au-Ligand Binding Energy BE (kcal/mol), the Au–Au Distance (\AA), and the Depiction of ENTO and HNTO of the Transition for Au_2L_2 with Various Ligands L^a

Ligand	%Au in ENTO/HNTO		Ω^1	f^1	BE	d(Au–Au)	ENTO	HNTO ^b
	Fragment	NBO						
-	100/100	100/100	3.14	0.000	-	2.512		
			3.15	0.272				
OPH ₃	70/97	66/94	4.72	0.518	16.5	2.501		
(CH ₃) ₂ O	95/99	86/97	4.76	0.443	12.4	2.498		
CH ₃ OH	92/96	86/96	4.07	0.418	13.4	2.498		
HCOOH	100/99	91/96	4.94	0.369	10.6	2.498		
H ₂ O	93/99	88/97	4.59	0.413	13.3	2.497		
NH ₃	100/86	90/80	4.96	0.259	23.7	2.512		
CH ₃ NH ₂	97/81	83/75	4.84	0.216	24.4	2.514		
H ₂ S	86/78	75/72	4.67	0.179	20.4	2.531		
(CH ₃) ₃ N	96/73	78/69	4.85	0.174	22.5	2.515		
CH ₃ SH	82/71	67/64	4.46	0.142	22.9	2.534		
(CH ₃) ₂ S	80/64	64/57	4.27	0.101	24.5	2.536		
PH ₃	78/73	62/63	4.06	0.084	28.7	2.564		
CH ₃ PH ₂	67/68	60/57	3.83	0.059	31.5	2.568		
C ₅ H ₅ N	30/70	25/64	5.02	0.048	23.3	2.513		

^aCalculations have been performed using TDDFT approach at CAM-B3LYP/TZVP level. ^bThe oscillator strength, the energy and ENTO/HNTO combinations for the first and the fourth (first allowed) lowest electronic transitions in Au_2 are presented.

atomic orbitals onto the antibonding combination of two 6s atomic orbitals of the internal Au_2 dimer. As a consequence, we expect Au_4 cluster to be nonemissive. The absorbance of the cluster is largely concentrated in a single peak at ~ 3 eV. This transition becomes the lowest upon Au_4 ligation in the $\text{Au}_4(\text{PH}_3)_2$ and $\text{Au}_4(\text{NH}_3)_2$ and, subsequently, both clusters should display strong fluorescence yield (Figure 3). The NTOs of the lowest optically active state are localized mostly on the nonligated Au atom pair (Table 1 and 1S of the SI). Similarly to the Au_2 description by CAM-B3LYP model, the ligation of Au_4 with two NH_3 or PH_3 ligands destabilizes symmetrical $P_x(6s)$ orbital of bare Au_4 . As such, the lowest transition in the ligated system, from $P_z(6s)$ to $D(6s)$, becomes allowed (Tables 1 and S1 and S3 of the SI). Although both electron and hole NTOs of this transition are primarily localized on outer gold atoms, the ENTOs also demonstrate significant involvement of 6s AOs of two internal gold atoms. Addition of two more ligands to form $\text{Au}_4(\text{PH}_3)_4$ and $\text{Au}_4(\text{NH}_3)_4$ molecules brings more changes in clusters' absorption spectra, with multiple peaks appearing in the wide region of $\sim 3\text{--}5$ eV (Figure 3). However, CAM-B3LYP model consistently predicts the lowest excited state in

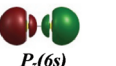
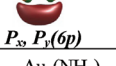
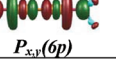
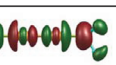
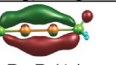
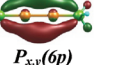
both $\text{Au}_4(\text{PH}_3)_4$ and $\text{Au}_4(\text{NH}_3)_4$ molecules (Figure 3) to be optically dark by symmetry, thus likely rendering these clusters to be nonemissive. The NTOs show that in this transition the electron density shifts from the peripheral Au–Au bonds to the center of the rhombus (Table 1).

The TPSS method displays mixed performance: its results are consistent with CAM-B3LYP modeling for all nonemissive systems (Au_4 , $\text{Au}_4(\text{PH}_3)_4$ and $\text{Au}_4(\text{NH}_3)_4$), where the lowest optically inactive state is predicted to be of the same type by both functionals. However, the TPSS description of possibly fluorescent clusters $\text{Au}_4(\text{PH}_3)_2$ and $\text{Au}_4(\text{NH}_3)_2$ is different. Contrary to CAM-B3LYP modeling, the lowest transition predicted by TPSS calculations originates from gold 5d AOs to $D(6s)$ and is expected to be optically dark. The respective NTOs clearly show vanishing overlap between electron and hole orbitals (Table 1), thus again emphasizing the charge transfer nature of this transition.

CONCLUSIONS

The ligand effects on the optical spectra of Au_2 and Au_4 clusters have been studied using TDDFT methodology. Our calcu-

Table 3. Transition Number, Energy Ω (eV), Oscillator Strength f and the Main Electron/Hole NTO Pair Contributing to the Absorption Transition in Spectra of Bare and Ligated Gold Dimer from CAM-B3LYP DFT Model^a

#	Ω	f	ENTO	HNTO	% contribution
Au ₂					
4	3.15	0.272			97.7
11,12*	5.54	0.434			96.4
Au ₂ (NH ₃) ₂					
1	4.96	0.259			98.0
5	5.25	0.260			69.0
10	5.68	0.647			65.3
Au ₂ (PH ₃) ₂					
5	5.48	0.572			79.0
13,14*	5.87	0.146			71.4
17	6.04	0.557			81.4
19	6.07	0.826			80.3

^aThe atomic orbital makeup of each NTO is indicated in parentheses next to the symbol of the cluster orbital. The last column shows the percent contribution of the main NTO pair into the absorption transition.

lations show that overall multiple excited states with large oscillator strength (mainly $S \rightarrow P_z$ or $S \rightarrow P_{x,y}$ excitations) contribute to the optical absorption of all considered clusters. To determine the fluorescence ability of these species, we rely on the Kasha's rule stating that the molecule should emit from its lowest excited state (whose oscillator strength defines fluorescence efficiency). Moreover, observed inconsistency between excited state description in TPSS and CAM-B3LYP functional models likely indicates failure of TPSS to describe the excited states with significant charge transfer character.^{48,49} Consequently, we count on CAM-B3LYP results to analyze trends in the excited state structure.

The cluster ligation eliminates the low-energy absorption peak of Au₂, whereas its high energy absorption peak remains intact. In agreement with preliminary experimental data^{45,47} the CAM-B3LYP results suggest that Au₂ and Au₂L₂ clusters with hard oxygen- or nitrogen-coordinating ligands should be fluorescent whereas clusters with soft phosphorus- or sulfur-coordinating ligands may show only a weak or vanishing emission. The calculated Au₄ absorption spectrum has only one significant absorption peak that slightly blue-shifts upon the cluster ligation. The ligand coordination also gives rise to

additional optically active states, thus, broadening the absorption spectra. CAM-B3LYP modeling predicts Au₄, Au₄(PH₃)₄ and Au₄(NH₃)₄ molecules likely to be nonemissive, whereas Au₄(PH₃)₂ and Au₄(NH₃)₂ should exhibit strong fluorescence. Thus ligand environment has strong effects on the linear absorption spectra and, particularly, on the fluorescence ability of small gold clusters, as captured by long-range corrected CAM-B3LYP kernel.

As commonly stated in the current literature, the modeling of complex metal or semiconductor systems (like metal clusters or metal chalcogenide nanocrystals) is conducted with simplified models of realistic ligands to minimize the computational cost. As current findings indicate, the nature of the chosen ligand might significantly alter the results of such calculations, especially if electronic properties of the system are of interest. Consequently, a justification of a particular ligand model choice is necessary to ensure that the results obtained on a model ligand system are transferrable onto realistic ligands. In the particular case of ligated gold clusters, it is important to point out that ligands might influence the absorption/emission properties of gold clusters not only via enabling the electron delocalization onto their orbitals thereby reducing the cluster's oscillator strength (as found for the ligated gold dimer), but via stabilization/destabilization of cluster's molecular orbitals, thereby changing the symmetry of the lowest electronic transition and significantly altering intensity of the electronic transition associated with those orbitals (e.g., in Au₄L₄ clusters). In the case of orbital stabilization/destabilization, the nature of the ligand might not be as crucial as in the case of metal-ligand electron delocalization. Semilocal TPSS DFT model lacks the long-range orbital exchange interaction and proved to be unreliable and inconsistent, frequently predicting optically forbidden excited states in the low energy region^{48,49} (in fact, none of the considered molecules should exhibit any emission in the TPSS description). Consequently, the usage of asymptotically corrected DFT models is suggested for proper excited state description of similar systems. It is also emphasized that selective ligation of gold clusters should potentially allow for control over the emission wavelength and its efficiency in these systems. Future detailed studies of excited state geometries and related Franck-Condon activities are necessary for quantitative assertion of photoluminescent properties of ligated gold clusters.

ASSOCIATED CONTENT

Supporting Information

Figure S1 showing frontier MO diagrams of partially ligated Au₄ cluster (Au₄(NH₃)₂); Table S1 displaying NTO plots of Au₂(PH₃)₂, Au₄(NH₃)₂ and Au₄(PH₃)₄ with DFT functionals TPSS and CAM-B3LYP in solvent; Tables S2 and S3 are presenting orbital makeup of strongest absorption transitions in bare and ligated gold dimers and tetramers, respectively. This material is available free of charge via the Internet at <http://pubs.acs.org>.

AUTHOR INFORMATION

Corresponding Author

*E-mail: ivanov@lanl.gov (S.A.I.); serg@lanl.gov (S.T.).

ACKNOWLEDGMENTS

This work was supported by the Los Alamos Directed Research and Development (LDRD) funds. We acknowledge support of

the Center for Nonlinear Studies (CNLS). This work was performed, in part, at the Center for Integrated Nanotechnologies, a U.S. Department of Energy, Office of Basic Energy Sciences User Facility. Los Alamos National Laboratory is operated by Los Alamos National Security, LLC, for the National Nuclear Security Administration of the U.S. Department of Energy under contract DE-AC52-06NA25396.

■ REFERENCES

- (1) Pyykkö, P. *Angew. Chem. Int. ed.* **2004**, *43*, 4412–4456.
- (2) Andres, R. P.; Bein, T.; Dorogi, M.; Feng, S.; Henderson, J. I.; Kubiak, C. P.; Mahoney, W.; Osifchin, R. G.; Reifenberger, R. *Science* **1996**, *272*, 1323–1325.
- (3) Collings, B. A.; Athanassenas, K.; Lacombe, D.; Rayner, D. M.; Hackett, P. A. *Opt.- J. Chem. Phys.* **1994**, *101*, 3506–3513.
- (4) Fedrigo, S.; Harbich, W.; Buttet, J. *J. Chem. Phys.* **1993**, *99*, 5712–5717.
- (5) Harbich, W.; Fedrigo, S.; Buttet, J.; Lindsay, D. M. Z. *Phys. D-At., Mol. Clusters* **1991**, *19*, 157–159.
- (6) Palpant, B.; Prevel, B.; Lerme, J.; Cottancin, E.; Pellarin, M.; Treilleux, M.; Perez, A.; Vialle, J. L.; Broyer, M. *Phys. Rev. B* **1998**, *57*, 1963–1970.
- (7) Wilcoxon, J. P.; Martin, J. E.; Parsapour, F.; Wiedenman, B.; Kelley, D. F. *J. Chem. Phys.* **1998**, *108*, 9137–9143.
- (8) Cleveland, C. L.; Landman, U.; Schaaff, T. G.; Shafiqullin, M. N.; Stephens, P. W.; Whetten, R. L. *Phys. Rev. Lett.* **1997**, *79*, 1873–1876.
- (9) Zheng, J.; Nicovich, P. R.; Dickson, R. M. *Annu. Rev. Phys. Chem.* **2007**, *58*, 409–431.
- (10) Zheng, J.; Petty, J. T.; Dickson, R. M. *J. Am. Chem. Soc.* **2003**, *125*, 7780–7781.
- (11) Das, K. K.; Balasubramanian, K. *J. Mol. Spectrosc.* **1990**, *140*, 280–294.
- (12) Lee, T. H.; Gonzalez, J. I.; Dickson, R. M. *Proc. Nat. Acad. Sc.* **2002**, *99*, 10272–10275.
- (13) Lerme, J.; Palpant, B.; Prevel, B.; Cottancin, E.; Pellarin, M.; Treilleux, M.; Vialle, J. L.; Perez, A.; Broyer, M. *Eur. Phys. D* **1998**, *4*, 95–108.
- (14) Link, S.; Beeby, A.; FitzGerald, S.; El-Sayed, M. A.; Schaaff, T. G.; Whetten, R. L. *J. Phys. Chem. B* **2002**, *106*, 3410–3415.
- (15) Pyykkö, P. *Chem. Soc. Rev.* **2008**, *37*, 1967–1997.
- (16) Zhao, J.; Yang, J.; Hou, J. G. *Phys. Rev. B* **2003**, *67*, 085404–085410.
- (17) Spivey, K.; Williams, J. I.; Wang, L. *Chem. Phys. Lett.* **2006**, *432*, 163–166.
- (18) Shafai, G.; Hong, S.; Bertino, M.; Rahman, T. S. *J. Phys. Chem. C* **2009**, *126*, 014704–014711.
- (19) Bravo-Pérez, G.; Garzón, I. L.; Novaro, O. *J. Mol. Struct.: THEOCHEM* **1999**, *493*, 225–231.
- (20) Wang, J.; Wang, G.; Zhao, J. *Phys. Rev. B* **2002**, *66*, 035418–035423.
- (21) Olson, R. M.; Varganov, S.; Gordon, M. S.; Metiu, H.; Chretien, S.; Piecuch, P.; Kowalski, K.; Kucharski, S. A.; Musial, M. *J. Am. Chem. Soc.* **2004**, *127*, 1049–1052.
- (22) Häkkinen, H.; Landman, U. *Phys. Rev. B* **2000**, *62*, 2287–2290.
- (23) Li, X. B.; Wang, H. Y.; Yang, X. D.; Zhu, Z. H.; Tang, Y. J. *J. Chem. Phys.* **2007**, *126*, 084505–084512.
- (24) Xiao, L.; Tollberg, B.; Hu, X.; Wang, L. *J. Chem. Phys.* **2006**, *124*, 114309–114318.
- (25) Daniel, M.-C.; Astruc, D. *Chem. Rev.* **2003**, *104*, 293–346.
- (26) Lecoultrre, S.; Rydlo, A.; Felix, C.; Harbich, W. *Eur. Phys. D* **2009**, *52*, 187–190.
- (27) Huang, T.; Murray, R. W. *J. Phys. Chem. B* **2001**, *105*, 12498–12502.
- (28) Jiang, D. E. *Acta Phys.-Chim. Sin.* **2010**, *26*, 999–1016.
- (29) Kryachko, E. S.; Remacle, F. *J. Chem. Phys.* **2007**, *127*, 194305–194315.
- (30) Molina, L. M.; Hammer, B. *Phys. Rev. Lett.* **2003**, *90*, 206102–206105.
- (31) Shafai, G. S.; Shetty, S.; Krishnamurti, S.; Shah, V.; Kanhere, D. *G. J. Chem. Phys.* **2007**, *126*, 12072–12078.
- (32) Goel, S.; Velizhanin, K. A.; Piryatinski, A.; Tretiak, S.; Ivanov, S. *A. J. Phys. Chem. Lett.* **2010**, *1*, 927–931.
- (33) Frisch, M. J. T., G. W.; Schlegel, H. B.; Scuseria, G. E.; Robb, M. A.; Cheeseman, J. R.; Montgomery, Jr., J. A.; Vreven, T.; Kudin, K. N.; Burant, J. C.; Millam, J. M., et al. *Gaussian 09 Revision A-2* 2009.
- (34) Schafer, A.; Horn, H.; Ahlrichs, R. *J. Chem. Phys.* **1992**, *97*, 2571–2577.
- (35) Tao, J. M.; Perdew, J. P.; Staroverov, V. N.; Scuseria, G. E. *Phys. Rev. Lett.* **2003**, *91*, 146401–146404.
- (36) Yanai, T.; Tew, D. P.; Handy, N. C. *Chem. Phys. Lett.* **2004**, *393*, 51–57.
- (37) Barone, V.; Cossi, M. *J. Phys. Chem. A* **1998**, *102*, 1995–2001.
- (38) Martin, R. L. *J. Chem. Phys.* **2003**, *118*, 4775–4777.
- (39) Stone, A. J. *Inorg. Chem.* **1981**, *20*, 563–571.
- (40) Balasubramanian, K.; Feng, P. Y.; Liao, M. Z. *J. Chem. Phys.* **1989**, *91*, 3561–3570.
- (41) Bishea, G. A.; Morse, M. D. *J. Chem. Phys.* **1991**, *95*, 5646–5659.
- (42) Fedrigo, S.; Harbich, W.; Buttet, J. *J. Chem. Phys.* **1993**, *99*, 5712–5717.
- (43) Vydrov, O. A.; Heyd, J.; Krukau, A.; Scuseria, G. E. *J. Chem. Phys.* **2006**, *125*, 074106–16.
- (44) Devadas, M. S.; Kim, J.; Sinn, E.; Lee, D.; Goodson, T. III; Ramakrishna, G. *J. Phys. Chem. C* **2010**, *114*, 22417–22423.
- (45) Yuping, B.; Chang, Z.; Vu, D. M.; Temirov, J. P.; Dyer, R. B.; Martinez, J. S. *J. Phys. Chem. C* **2007**, *111* (33), 12194–12198.
- (46) Muhammed, M. A. H.; Ramesh, S.; Sinha, S. S.; Pal, K. S.; Pradeep, T. *Nano Res.* **2008**, *1*, 333–340.
- (47) Bao, Y.; Yeh, H.-C.; Zhong, C.; Ivanov, S. A.; Sharma, J. K.; Neidig, M. L.; Vu, D. M.; Shreve, A. P.; Dyer, R. B.; Werner, J. H.; et al. *J. Phys. Chem. C* **2010**, *114* (38), 15879–15882.
- (48) Magyar, R. J.; Tretiak, S. *J. Chem. Theory Comput.* **2007**, *3*, 976–987.
- (49) Dreuw, A.; Head-Gordon, M. *Chem. Rev.* **2005**, *105*, 4009–4037.